Modeling oxygen transport in surgical tissue transfer

Anastasios Matzavinos[a], Chiu-Yen Kao[b,c], J. Edward F. Green[c], Alok Sutradhar[d], Michael Miller[d], and Avner Friedman[b,c,1]

[a]Department of Mathematics, Iowa State University, Ames, IA 50011; [b]Department of Mathematics, Ohio State University, Columbus, OH 43210; [c]Mathematical Biosciences Institute, Ohio State University, Columbus, OH 43210; and [d]Division of Plastic Surgery, Ohio State University Medical Center, Columbus, OH 43210

Contributed by Avner Friedman, May 14, 2009 (sent for review November 7, 2008)

Reconstructive microsurgery is a clinical technique used to transfer large amounts of a patient's tissue from one location used to another in order to restore physical deformities caused by trauma, tumors, or congenital abnormalities. The trend in this field is to transfer tissue using increasingly smaller blood vessels, which decreases problems associated with tissue harvest but increases the possibility that blood supply to the transferred tissue may not be adequate for healing. It would thus be helpful to surgeons to understand the relationship between the tissue volume and blood vessel diameter to ensure success in these operations. As a first step towards addressing this question, we present a simple mathematical model that might be used to predict successful tissue transfer based on blood vessel diameter, tissue volume, and oxygen delivery.

reconstructive surgery | surgical flap | ischemia | porous media | PDE model

Reconstructive surgery is a specialized form of plastic surgery that frequently involves moving a patient's tissue from one location to another in discreet units known as surgical flaps. Originally, actual flaps of skin were elevated and rotated into position. Over time, however, the definition of a flap broadened to include any tissue transferred with preservation of its blood supply. The vessels that supply blood to the flap are called the vascular pedicle. Throughout the body, there are units of muscle, skin, fat, bone, viscera, and combinations thereof that can be isolated on single arteries and veins as surgical flaps. If the distance from the original location of the flap to the area needing reconstruction is less than the length of the vascular pedicle, then the tissue can be rotated without disrupting the blood supply. For greater distances, the pedicle vessels must be divided and reattached to the patient's arteries and veins in the area of reconstruction. Usually these vessels are <5 mm in diameter, and microvascular surgery is performed by using an operating microscope and specialized instruments to reattach the vessels and restore blood supply to the flap. A flap transferred in this way is known as a free flap because, during transfer, the tissues are completely detached from, or free of, the patient. The trend in reconstructive microsurgery is to transfer free flaps using smaller and smaller blood vessels.

Breast reconstructive surgery provides a good illustration of the evolution of these techniques. Abdominal tissue is ideal for breast reconstruction. Techniques used to transfer surgical flaps composed of skin and fat from the lower abdomen to the chest were introduced by Hartrampf and colleagues in 1982 (1). The blood supply to the tissues was provided by multiple small blood vessels arising from larger source vessels running the length of the rectus abdominis muscle, a major muscle oriented vertically on the abdominal wall between the ribs and the pelvis bone. A large portion of tissue could be rotated to the chest by maintaining the attachments of the rectus abdominis muscle at the rib margin to preserve the blood supply to the tissue. Although a generally successful technique still in wide use today, it is often associated with wound-healing problems due to inadequate blood supply to the tissue flap. Microsurgical transfer of the lower abdominal tissue was introduced to try to overcome this problem. This method allows the tissue to be transferred by using the more reliable inferior blood supply source. Despite these advantages, this procedure was still associated with complications related to disruption of the abdominal wall muscles. This difficulty led to introduction of a surgical flap based only on the blood vessels that pass through the muscles called perforating vessels. Flaps were designed that required the surgeon to select a single perforating vessel and follow it through the muscle without including any muscle in the flap for transfer. The perforating vessels have luminal diameters ranging from several hundred microns up to as much as 1.5 mm. The surgeon must make a decision to transfer the flap based on one or more of these vessels. If the blood supply provided by the perforating vessels is inadequate, then some portion, or even the entire flap, will be lost. There is no objective method currently available to assist the surgeon in making this decision.

It is reasonable to postulate that a relationship exists between the volume of blood flow through the perforating vessels and the volume of tissue that may be reliably supported by it. There is no routine clinical method for the surgeon to directly assess blood-flow volume through the small perforating blood vessels during surgery, but blood vessel diameter can be assessed. If the relationship between the diameter of the perforating blood vessels and the volume of tissue intended for transfer was understood, then more reliable surgery would be possible, reducing morbidity and cost.

Flow of blood and delivery of oxygen within a tissue is an area of intense research activity. However, it is extremely difficult to simulate computationally due to the complex branching geometry of the blood vessels and the range of sizes of vessels involved. At the larger end of the scale, flows through branching vessels have been studied extensively (2–4). These studies tend to neglect the smaller vessels, which are important for the delivery of oxygen in a tissue. At the capillary scale, detailed experimental and simulation studies of flows in the microvasculature have been carried out (5–9), taking into account such factors as changes in the blood's apparent viscosity with vessel diameter, and separation of red blood cells and plasma at bifurcations. However, it is not currently practical to image the smallest vessels in a clinical setting, and even if it were, it would be extremely computationally expensive to determine the flow. Hence, in this paper we pursue a simpler strategy of treating blood flow through the vascular network as being akin to fluid flow through a porous medium. On a smaller scale, this approach was used by Pozrikidis, et al. (10) to describe fluid flow within a solid tumor. More recent work by Chapman, et al. (11) extended this approach to consider flow through a rectangular grid of capillaries within a tumor. Here, again, the interstitium was assumed to be an isotropic porous medium, and Poiseuille flow was assumed in the capillaries. Through the application of homogenization techniques, it was found that on the lengthscale of the tumor (*i.e.* a lengthscale much longer than the typical capillary separation) the behavior of the capillary bed was also effectively that of a porous medium. A more phenomenological approach was taken by Breward, et al. (12), who developed a multiphase model describing vascular tumor growth. Here, the tumor is composed of a mixture of tumor cells, extracellular material (mainly

Author contributions: A.M., C.-Y.K., J.E.F.G., A.S., M.M., and A.F. designed research, performed research, and wrote the paper.

The authors declare no conflict of interest.

[1]To whom correspondence should be addressed. E-mail: afriedman@mbi.ohio-state.edu.

This article contains supporting information online at www.pnas.org/cgi/content/full/0905037106/DCSupplemental.

water) and blood vessels, with the model being used to investigate the impact of angiogenesis, or blood vessel occlusion on tumor growth. A similar model was used by O'Dea, et al. (13) to describe tissue growth in a perfusion bioreactor.

The aim of the present paper is to develop a mathematical model that allows us to estimate the level of oxygenation in a tissue given its size and shape and the diameter of the perforating artery. The model could provide a useful tool for determining the size of the free flap that can be successfully transferred in a reconstructive microsurgical procedure. However, careful validation of the model predictions and determination of parameter values are necessary before the model can be used as a predictive tool.

Mathematical Model

We adopt a multiphase approach, similar to that used in refs. 12, and assume that the tissue consists of live tissue cells, arterial blood vessels, and venous blood vessels, with volume fractions $\theta_c(\boldsymbol{x})$, $\theta_a(\boldsymbol{x})$ and $\theta_v(\boldsymbol{x})$ respectively. (The volume fractions are defined by using the volume-averaging procedure described in refs. 14.) It is assumed that there are no voids, that is

$$\theta_a + \theta_c + \theta_v = 1, \qquad [1]$$

and that the tissue cells are immobile, whereas in the arteries and veins blood flows with velocities $\boldsymbol{v}_a$ and $\boldsymbol{v}_v$, respectively. The blood flow is driven by gradients in the arterial and venous pressures, denoted respectively p_a and p_v. Blood moves from the arterial to the venous system at a rate which is assumed to be proportional to the product of the 2 volume fractions and the pressure difference. Conservation of mass of arterial and venous blood then yields the following equations:

$$\nabla \cdot (\theta_a \boldsymbol{v}_a) = -\lambda_1^* \theta_a \theta_v (p_a - p_v), \qquad [2]$$

$$\nabla \cdot (\theta_v \boldsymbol{v}_v) = \lambda_1^* \theta_a \theta_v (p_a - p_v), \qquad [3]$$

where λ_1^* is the rate of transfer of blood from the arterial to the venous systems.

Several studies have considered the problem of blood flow through small vessels and its effect on oxygen or drug delivery to tumors (7–9). These involve detailed computational modeling of the geometry of vessels and their evolution over time in response to angiogenic factors secreted by the tumor. They also take the complex rheology of blood into account by introducing an effective blood viscosity which depends on the haematocrit (volume fraction of blood cells) and the vessel radius. However, the phenomenological relation for blood viscosity is based on the assumption of Poiseuille flow, but in reality the velocity profile, particularly in the smaller vessels, is not parabolic but blunted (15). Another complicating factor is the fact that tumor vasculature is not typical of that in noncancerous tissues (16). An alternative approach uses homogenization techniques to obtain a macroscopic description for the case of Poiseuille flow through a rectangular grid of capillaries of constant, identical diameter (11). In this paper, flow of blood through the vasculature is treated as the flow of fluid through an isotropic porous medium, which has been shown to be a valid macroscopic approximation for the case of Poiseuille flow through a square grid of capillaries of constant, identical diameter (11). Although this is a very simplified assumption concerning the capillary network, in the absence of detailed information about the geometry of the vasculature, we believe our model provides a useful and tractable first approximation of the true situation.

Under the assumptions stated above, the blood velocities obey Darcy's law

$$-\kappa_a^* \nabla p_a = \theta_a \boldsymbol{v}_a, \qquad [4]$$

$$-\kappa_v^* \nabla p_v = \theta_v \boldsymbol{v}_v, \qquad [5]$$

where κ_a^* and κ_v^* are the permeabilities of the tissue to arterial and venous blood, respectively, and give a measure of the resistance of the vascular networks. These values are, in practice, likely to vary within the tissue, due to variations in the average diameter of the vessels. In particular, regions with more large vessels will have lower resistance, which might suggest that the permeabilities should be increasing functions of the relevant volume fraction. However, for simplicity we assume that they are constants. Combining Eq. **2** with Eq. **3** and Eq. **4** with Eq. **5** results in the following equations for the pressures

$$\kappa_a^* \nabla^2 p_a = \lambda_1^* \theta_a \theta_v (p_a - p_v), \qquad [6]$$

$$\kappa_v^* \nabla^2 p_v = -\lambda_1^* \theta_a \theta_v (p_a - p_v). \qquad [7]$$

Note the similarity between the form of the above equations and that for the capillary pressure obtained by Chapman et al. (11) (their equation 65), which provides some support for our choice of functional form for the terms on the right-hand side.

The oxygen concentrations (per unit volume of constituent) in the cells and the arterial and venous blood are denoted by $c_c(\boldsymbol{x}, t)$, $c_a(\boldsymbol{x}, t)$, and $c_v(\boldsymbol{x}, t)$, respectively. Oxygen diffuses within the tissue with diffusion coefficient D_c^* (note that we have scaled the diffusive flux by the volume fraction, as in refs. 17), and is assumed to be consumed by the cells at a constant rate ν^*. The equation for c_c is then

$$\frac{\partial}{\partial t}(\theta_c c_c) = D_c^* \nabla \cdot (\theta_c \nabla c_c) + \lambda_2^* \theta_a \theta_c (c_a - c_c) + \lambda_3^* \theta_v \theta_c (c_v - c_c) - \nu^* \theta_c c_c. \qquad [8]$$

Oxygen in the blood is transported by the flow, and may diffuse within the fluid. However, there are a number of complicating factors which need to be considered. One is flow-induced dispersion. The case of Poiseuille flow in a straight tube, giving some insight for an individual blood vessel, was studied by Taylor (18), who found an increase in the apparent diffusivity of the solute within the fluid, due to the velocity profile being parabolic across the vessel. (However, as noted above, the blood is a non-Newtonian fluid, and hence the velocity profile is not parabolic but blunted (15), which will affect the degree of dispersion.) Flow-induced dispersion in porous media has been extensively studied (19–22) and manifests itself as an enhanced, anisotropic diffusivity of the solute. In the case of media with a periodic microstructure, the dispersion tensors, which depend on the microscopic (i.e. vessel-scale) geometry and flow velocity, can be calculated explicitly (20, 21, 23, 24). An alternative approach, based on volume averaging, was used by Whitaker (22) to show that for an isotropic medium the additional diffusive effects are governed by 2 parameters. His technique does not provide an expression for these, but he suggests that they might be determined experimentally. Complications also arise from the binding and unbinding of oxygen to hemoglobin, again resulting in nonlinear diffusion (6). However, for the sake of simplicity and because the structure of the vasculature is not known, we neglect these complexities, and assume constant effective diffusion coefficients D_a^* and D_v^* for oxygen in the arterial and venous blood, respectively. The effect of changing these coefficients will be discussed in the section on *Simulation Results*.

In addition to the effects metioned above, there is a flux of oxygen from the blood into the cells at a rate proportional to the difference in the oxygen concentrations and to the degree of proximity between the vasculature and the tissue cells (modeled as proportional to the product of the volume fractions). Finally, oxygen in arterial blood is lost when the blood moves to the venous system. Thus, the following equations for c_a and c_v are obtained:

$$\frac{\partial}{\partial t}(\theta_a c_a) + \nabla \cdot (c_a \theta_a \boldsymbol{v}_a) = D_a^* \nabla \cdot (\theta_a \nabla c_a) - \lambda_1^* c_a \theta_a \theta_v (p_a - p_v) - \lambda_2^* \theta_a \theta_c (c_a - c_c), \qquad [9]$$

Table 1. Boundary conditions

Variable	Perforating blood vessels	On the remaining part
p_a	$p_a = p_a^0$	$n \cdot \nabla p_a = 0$
p_v	$p_v = p_v^0 = 0$	$n \cdot \nabla p_v = 0$
c_a	$c_a = c_a^0$	$n \cdot (-D_a^* \nabla c_a + c_a \boldsymbol{v}_a) = 0$
c_v	$c_v = c_v^0$	$n \cdot (-D_v^* \nabla c_v + c_v \boldsymbol{v}_v) = 0$
c_c	$n \cdot \nabla c_c = 0$	$n \cdot \nabla c_c = 0$

$$\frac{\partial}{\partial t}(\theta_v c_v) + \nabla \cdot (c_v \theta_v \boldsymbol{v}_v) = D_v^* \nabla \cdot (\theta_v \nabla c_v) + \lambda_1^* c_a \theta_a \theta_v (p_a - p_v) - \lambda_3^* \theta_v \theta_c (c_v - c_c), \quad [10]$$

where λ_2^* and λ_3^* are the volume-averaged oxygen permeability coefficients of the arterial and venous blood vessels.

The model thus consists of the 5 equations (Eqs. **6**–**10**), for p_a, p_v c_a, c_v, and c_c, which are to be solved subject to initial conditions for the oxygen concentrations c_a, c_v, and c_c, and boundary conditions given in Table 1 for all 5 variables. (Note that we can set $p_v^0 = 0$ without loss of generality, as pressures are unique only up to an additive constant.) For simplicity, the model is developed for a flap with rectangular geometry as illustrated in Fig. 1: The upper layer, consisting of the dermis, the epidermis, and the subdermal plexus is 2 mm thick, whereas the fat layer is $b = 8$ mm thick, and the ratio c/a of length to width is between 1.5 and 3. Parameter values are given in Table 2 and, for simplicity, since λ_3^* is very small, we take it to be zero.

Nondimensionalization. The mathematical model contains a representative lengthscale L based on the size of the tissue, which is approximately 4–10 cm, and a pressure scale p_a^0 is based on the typical pressure drop between large arteries and large veins. The velocity scale U is the typical rate of blood flow through the tissue, which is related to the pressure scale, lengthscale, and tissue porosity. The model has 2 timescales, the time taken for blood to traverse the tissue, (L/U), and the time for oxygen supply to the cells through the arterial wall, $(1/\lambda_2^*)$. Oxygen concentrations are scaled with the typical value for arterial blood, C^*. Thus,

$$t = \frac{1}{\lambda_2^*}\tilde{t},\ \boldsymbol{x} = L\tilde{\boldsymbol{x}},\ (c_a, c_c, c_v) = C^*(\tilde{c}_a, \tilde{c}_c, \tilde{c}_v),$$
$$(p_a, p_v) = p_a^0(\tilde{p}_a, \tilde{p}_v),\ (\boldsymbol{v}_a, \boldsymbol{v}_v) = U(\tilde{\boldsymbol{v}}_a, \tilde{\boldsymbol{v}}_v)$$

where the tildes indicate dimensionless quantities.

By choosing the velocity scale $U = \kappa_a^* p_a^0 / L$ and dropping the tildes to simplify notation, Eqs. **4** and **5** become

$$-\nabla p_a = \theta_a \boldsymbol{v}_a, \quad [11]$$

$$-\kappa \nabla p_v = \theta_v \boldsymbol{v}_v, \quad [12]$$

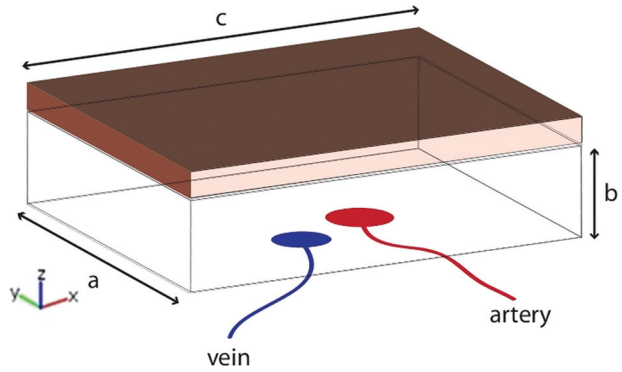

Fig. 1. Schematic of tissue flap. The top, colored layer consists of the dermis, epidermis, and subdermal plexus. The bottom layer represents fat tissue. The perforator artery and vein are located at the bottom of the flap.

Table 2. Parameter values

Parameter	Value	References
C^*	9.3×10^{-3} M	28
p_a^0	100 mm Hg	29
p_v^0	0 mm Hg	30
ν^*	10^{-3} sec^{-1}	(estimated)
$\lambda_1^* = \lambda_2^*$	8.2×10^{-3} sec^{-1}	(estimated)
λ_2^*	8.2×10^{-3} sec^{-1}	31
κ_a^*	$10^{-11} - 10^{-7}$ kg^{-1} m^3 s^1	32
κ_v^*	$10^{-11} - 10^{-7}$ kg^{-1} m^3 s^1	32
D_a^*	2.4×10^{-5} cm^{-2} sec^{-1}	(based on value for water)
D_v^*	2.4×10^{-5} cm^{-2} sec^{-1}	(based on value for water)
D_c^*	2.0×10^{-5} cm^{-2} sec^{-1}	33

where $\kappa = \kappa_v^*/\kappa_a^*$ is the effective permeability of the veins relative to the arteries. Substituting Eqs. **11** and **12** into Eqs. **6** and **7** yields

$$\nabla^2 p_a = \lambda_1 \theta_a \theta_v (p_a - p_v), \quad [13]$$

$$\kappa \nabla^2 p_v = -\lambda_1 \theta_a \theta_v (p_a - p_v), \quad [14]$$

where $\lambda_1 = \lambda_1^* p_a^0 L/U$.

The dimensionless version of Eqs. **8**–**10** are then

$$\frac{\partial}{\partial t}(\theta_c c_c) = D_c \nabla \cdot (\theta_c \nabla c_c) + \theta_a \theta_c (c_a - c_c) + \lambda_3 \theta_v \theta_c (c_v - c_c) - \nu \theta_c c_c, \quad [15]$$

$$\varepsilon \frac{\partial}{\partial t}(\theta_a c_a) + \nabla \cdot (c_a \theta_a \boldsymbol{v}_a) = \mathcal{P}^{-1} \nabla \cdot (\theta_a \nabla c_a) - \varepsilon \theta_a \theta_c (c_a - c_c) - \lambda_1 c_a \theta_a \theta_v (p_a - p_v), \quad [16]$$

$$\varepsilon \frac{\partial}{\partial t}(\theta_v c_v) + \nabla \cdot (c_v \theta_v \boldsymbol{v}_v) = D_v \mathcal{P}^{-1} \nabla \cdot (\theta_v \nabla c_v) - \varepsilon \lambda_3 \theta_v \theta_c (c_v - c_c) + \lambda_1 c_a \theta_a \theta_v (p_a - p_v), \quad [17]$$

with the following dimensionless parameters: $\varepsilon = \lambda_2^* L/U$, the ratio of blood-flow timescale to the oxygen-uptake timescale; $\mathcal{P}$, the effective Péclet number $\mathcal{P} = UL/D_a^*$ (the ratio of advective to diffusive transport) for oxygen in the blood; $D_v = D_v^*/D_a^*$, the relative diffusivity of oxygen in venous compared with arterial blood [since both types of blood consist mainly of water, one expects $D_v \sim O(1)$]; $\lambda_3 = \lambda_3^*/\lambda_2^*$, the relative rate of oxygen transfer from venous blood into the tissue compared with that from arterial blood; $D_c = D_c^*/\lambda_2^* L^2$, the ratio of the timescale of oxygen diffusion through the tissue to that for oxygen supply through the arterial wall; and $\nu = \nu^*/\lambda_2^*$, the rate of oxygen consumption by the cells relative to the rate of supply from the arteries.

The equations are to be solved in the 3-dimensional domain Ω (shown in Fig. 1). It is known that there is a higher density of blood vessels in the dermal region compared with the underlying layers of fat cells in the flap, and hence θ_a and θ_v will depend on z. In the following simulations, we set

$$\theta_a = \theta_v = 0.025 \left(\frac{2}{\pi} \arctan 100(z - 0.8) \right) + 0.075, \quad [18]$$

that is, θ_a and θ_v are approximately 0.05 in the layer of fat cells and 0.1 in the dermal region, respectively. The nondimensionalized boundary conditions at the perforating blood vessel are given by $p_a = 1$, $p_v = 0$, $c_a = 1$, $c_v = 0.2$, and $n \cdot \nabla c_c = 0$, but on the remainder of the boundary they take the same form as the corresponding dimensional conditions. For the sake of simplicity, it

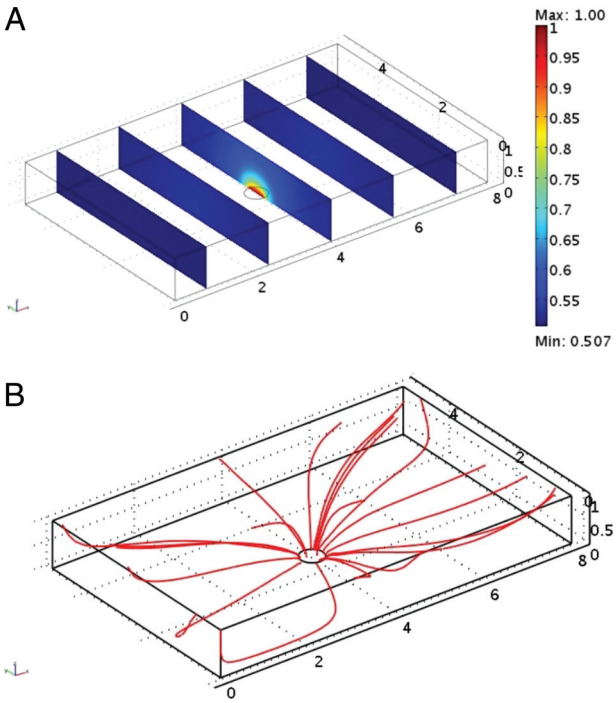

Fig. 2. Figures showing (*A*) the (nondimensionalized) distribution of the arterial blood pressure and (*B*) the corresponding pressure streamlines. According to Darcy's law, the pressure streamlines indicate blood-flow trajectories. The flap dimensions are 8 cm × 5 cm × 1 cm.

is assumed that the perforator artery and vein coincide in space and are represented by a circular area located at the center of the lower boundary of Ω. This assumption is reasonable, as the perforator artery and vein are usually very close to each other. The dimensional and dimensionless diameters of this circular domain are denoted by d and d_a respectively.

The initial conditions are

$$c_a(\boldsymbol{x},0)=0, c_v(\boldsymbol{x},0)=0, \text{ and } c_c(\boldsymbol{x},0)=0, \qquad [19]$$

for all $\boldsymbol{x}$ in the flap. The above represent an initially ischemic flap, which is perforated at $t=0$.

Methods

The system under consideration comprises the dimensionless Eqs. **11**–**17**, subject to the boundary and initial conditions stated above. The simulations were performed using the COMSOL Multiphysics software package. Our numerical implementation used a finite element space based on linear Lagrange elements. The mesh consisted of around 2,000 tetrahedral elements, varying according to the different geometries considered, and the finite element discretization was combined with a time integration in a method-of-lines approach.

Simulation Results

Figs. 2 and 3 are simulation results corresponding to a tissue flap of dimensions 8 cm × 5 cm × 1 cm. Fig. 3*A* and *B* show, respectively, the arterial pressure distribution and blood-flow trajectories. Similar computations have been performed for the venous pressure distribution. Fig. 3*A* and *B* show the corresponding (nondimensional) oxygen distribution in arteries and tissue, respectively. As can be seen from Fig. 3, the oxygen concentration in the tissue

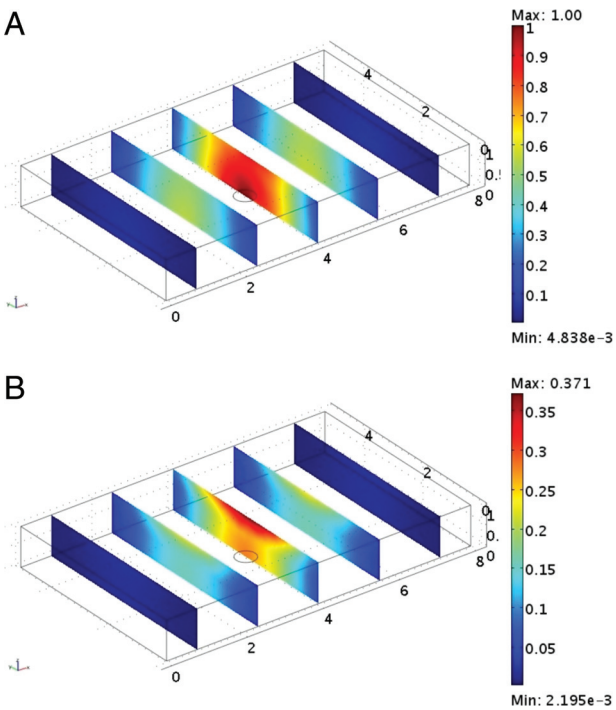

Fig. 3. Oxygen distribution in (*A*) artery blood and (*B*) in tissue after 4 hours of tissue reperfusion in the case of the large tissue flap (dimensions: 8 cm × 5 cm × 1 cm). As can be seen, in accordance with clinical observations, the flap develops fat necrosis away from the dermis layer.

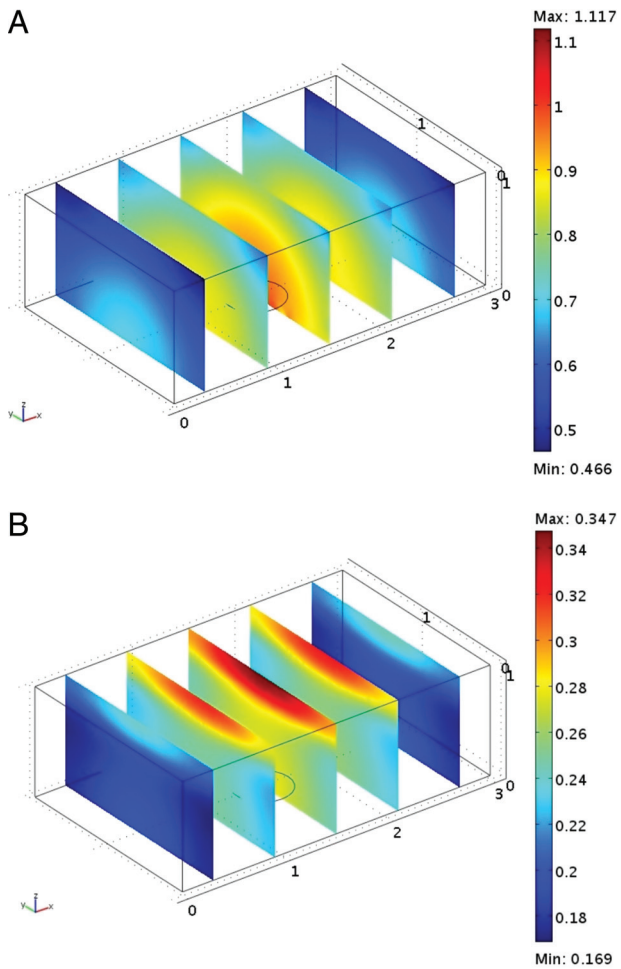

Fig. 4. Oxygen distribution in artery blood (*A*) and in tissue (*B*) after 4 hours of tissue reperfusion in the case of the small tissue flap (dimensions: 3 cm × $\frac{15}{8}$ cm × 1 cm). In this case, the perforator artery is successful in oxygenating the flap, as no fat necrosis develops.

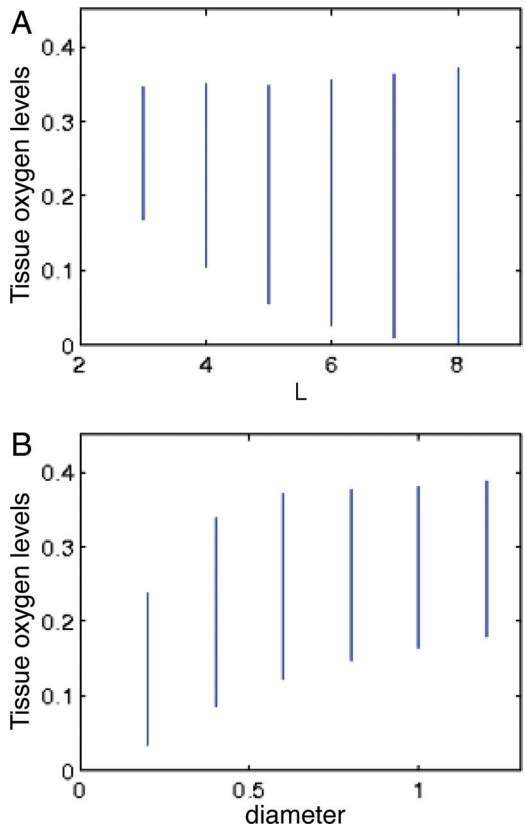

Fig. 5. Tissue oxygen concentration for flaps of different size and of different arterial diameter. (*A*) Range of oxygen concentration in the flaps with fixed ratio in the directions of x and y, when the longest length *L* varies between 3 cm and 8 cm. (*B*) Range of oxygen concentration in the flap of dimensions 4 cm × 2.5 cm × 1 cm with different arterial diameter ranging 0.2 cm to 1.2 cm.

drops below 5% of the oxygen concentration in arteries in certain tissue regions. This level of drop in oxygen availability is the hallmark of ischemia, and the tissue regions that experience it will eventually become necrotic. Owing to the denser vasculature in the dermis layer, most of the ischemic regions develop away from the dermis, resulting in fat necrosis. This finding is in agreement with clinical observations.

Fig. 4 shows the simulation results of oxygen distribution in artery blood (*A*) and tissue (*B*) of reperfusing a smaller tissue flap of dimensions 3 cm × $\frac{15}{8}$ cm × 1 cm with the same diameter of perforator artery as in Fig. 3. In this case, the oxygen concentration throughout the tissue is 15–19% of the normal oxygen concentration in arteries. This range corresponds to healthy physiological values of oxygen concentration in tissue and, hence, in this numerical experiment, the perforator used has been successful in adequately oxygenating the flap.

The range of oxygen concentrations can similarly be computed for flaps of any dimension and any diameter of artery. In Fig. 5*A* we consider flaps with fixed thickness 1 cm, fixed ratio of the horizontal lengths 8:5 and fixed arterial diameter of 5 mm. Fig. 5*A* shows how the range of oxygen concentration in the tissue varies as a function of the longer length *L*. In Fig. 5*B*, the flap dimensions are fixed at 4 cm × 2.5 cm × 1 cm although the diameter of the perforator artery varies. The flap may develop fat necrosis if the oxygen concentration goes below 0.15, or 15% of the oxygen concentration in the artery.

We investigated the effect of increasing the diffusion coefficients for oxygen in the blood (thus giving different values of $\mathcal{P}$ in Eqs. **16** and **17**), so as to give some qualitative insight into the possible effects of flow-induced dispersion. As seen in Figs. S7-S10 of the *SI Appendix*, the qualitative features of the previous simulations are not affected by increasing the diffusion coefficients.

Discussion

A fundamental problem in reconstructive surgery concerns how to determine the size of a flap that can be transferred without the development of necrosis. Improved understanding of the anatomy of tissue blood supply combined with advances in instrumentation and techniques has resulted in modern methods to transfer tissue based on single arteries and veins. The current challenge is intraoperative flap design. Surgeons must still rely on personal experience to make a qualitative assessment of the adequacy of blood supply when deciding how large to make the flap. If unsuccessful, the blood supply will be inadequate for the amount of tissue transferred, and portions of the flap will not survive. This can result in significant postoperative complications, additional surgery, increased morbidity, and increased medical costs. It is therefore important to develop a practical clinical tool to enable the most reliable flap design based on the adequacy of blood supply.

In this paper, we have demonstrated how a simple mathematical model might be used to address this important longstanding problem. We have shown how the minimum oxygen concentration in the tissue varies nonlinearly with the flap size and artery diameter, which would in principle allow the surgeon to predict whether a given flap/artery combination would develop necrosis. Our simulations are in qualitative agreement with clinical observations that flaps which are made too large first begin to develop necrosis at the edges. However, the present results should be seen in the spirit of a "proof of concept" study. We have mainly considered the simplest possible case, a cuboid geometry, where there is no anisotropy of the blood vessel network, and no variation in the oxygen transfer coefficients (although in the *SI Appendix*, we considered a simple example in which the latter assumption was relaxed). However, these limitations can be overcome, as discussed in *Mathematical Model*. Another extension to the model would be to include the effects of stresses within the tissue exerted by the extracellular matrix, which could result in the collapse of vessels and hence impede blood flow. This phenomenon could be incorporated into the current modeling framework by considering the momentum balance on the tissue cells, as in refs. 25. We also note that at later times, cell necrosis and vascular remodeling will become important, as the transferred tissue either becomes, or fails to become, integrated into the body in its new location. However, here we have considered a timescale of just a few hours after operation, which is insufficient for these effects to manifest themselves.

Before the model can become a predictive tool, careful validation of our predictions and determination of parameter values (e.g. by use of in vitro experiments) will be necessary. The improved model could then be used to make predictions of the expected reliability of surgical flaps based on a particular combination of artery and flap geometry. Eventually, it might become practical to gather enough data on individual patients to make patient-specific predictions. Emerging techniques in noninvasive, 3-dimensional imaging of blood vessel anatomy, such as computed tomography angiography (CTA), will no doubt prove useful. CTA allows the localization of blood vessels <1 mm in diameter (26). This detailed imaging, combined with a predictive model of the volume of tissue that might be transferred based on such vessels, would be an extremely valuable tool for surgical planning. The mathematical equations might also be more generally applied to tissues of all types that are affected by disorders related to ischemia, such as cardiac disease and stroke, which accounted for 35% of all deaths in the United States in 2005 (27).

ACKNOWLEDGMENTS. This work was supported by the National Science Foundation under Agreement No. 0112050. C.-Y. K was partially supported by National Science Foundation Grant DMS-0811003.

1. Hartrampf C, Scheflan M, Black P (1982) Breast reconstruction with a transverse abdominal island flap. *Plast Reconstr Surg* 69:216–225.
2. Bowles RI, Dennis SCR, Purvis R, Smith FT (2005) Multi-branching flows from one mother tube to many daughters or to a network. *Philos Trans R Soc London Ser A* 363:1045–1055.
3. Smith FT, et al. (2003) Fluid flow through various branching tubes. *J Eng Math* 47:277–298.
4. Smith FT, Jones MA (2003) AVM modelling by multi-branching tube flow: Large flow rates and dual solutions. *Math Med Biol* 20:183–204.
5. Pries AR, Secomb TW, Gaehtgens P (1996) Biophysical aspects of blood flow in the microvasculature. *Cardiovasc Res* 32:654–667.
6. Goldman D, Popel AS (2000) A computational study of the effect of capillary network anastomoses and tortuosity on oxygen transport. *J Theor Biol* 206:181–194.
7. Anderson ARA, Chaplain MAJ (1998) Continuous and discrete mathematical models of tumor-induced angiogenesis. *Bull Math Biol* 60:857–899.
8. McDougall SR, Anderson ARA, Chaplain MAJ, Sherratt JA (2002) Mathematical modelling of flow through vascular networks: Implications for tumor-induced angiogenesis and chemotherapy strategies. *Bull Math Biol* 64:673–702.
9. Stephanou A, McDougall SR, Anderson ARA, Chaplain MAJ (2006) Mathematical modelling of the influence of blood rheological properties upon adaptive tumor-induced angiogenesis. *Math Comput Model* 44:96–123.
10. Pozrikidis C, Farrow DA (2003) A model of fluid flow in solid tumors. *Ann Biomed Eng* 31:181–194.
11. Chapman SJ, Shipley RJ, Jawad R (2008) Multiscale modelling of fluid transport in tumors. *Bull Math Biol* 70:2334–2357.
12. Breward CJW, Byrne HM, Lewis CE (2003) A multiphase model describing vascular tumor growth. *Bull Math Biol* 65:609–640.
13. O'Dea RD, Waters SL, Byrne HM (2008) A two-fluid model for tissue growth within a dynamic flow environment. *Eur J Appl Math* 19:607–634.
14. Drew DA (1983) Mathematical modeling of two-phase flow. *Annu Rev Fluid Mech* 15:261–291.
15. Alonso C, Pries AR, Kiesslich O, Lerche D, Gaehtgens P (1995) Transient rheological behaviour of blood in low shear tube flow: velocity profiles and effective viscosity. *Am J Physiol Heart Circ Physiol* 268:25–32.
16. Jain RK (2005) Normalization of tumor vasculature: An emerging concept in antiangiogenic therapy. *Science* 307:58–62.
17. Cogan NG, Keener JP (2004) The role of biofilm matrix in structural development. *Math Med Biol* 21:147–166.
18. Taylor GI (1953) Dispersion of soluble matter in solvent flowing slowly through a tube. *Proc R Soc London Ser A* 219:186–203.
19. Saffman PG (1959) A theory of dispersion in a porous medium. *J Fluid Mech* 6:321–349.
20. Brenner H (1980) Dispersion resulting from flow through spatially periodic porous media. *Proc R Soc London Ser A* 297:81–133.
21. Salles J, et al. (1993) Taylor dispersion in porous media. Determination of the dispersion tensor. *Phys Fluids A* 5:2348–2376.
22. Whitaker S (1967) Diffusion and dispersion in porous media. *AIChE J* 13:420–427.
23. Rubenstein J, Mauri R (1986) Dispersion and convection in periodic porous media. *SIAM J Appl Math* 46:1018–1023.
24. Auriault JL, Adler PM (1995) Taylor dispersion in porous media: Analysis by multiple scale expansions. *Adv Water Res* 18(4):217–226.
25. Tosin A, Ambrosi D, Preziosi L (2006) Mechanics and chemotaxis in the morphogenesis of vascular networks. *Bull Math Biol* 68:1819–1836.
26. Phillips T, Stella D, Rozen W, Ashton M, Taylor G (2008) Abdominal wall CT angiography: A detailed account of a newly established preoperative imaging technique. *Radiology* 249:32–44.
27. Kung H, Hoyert D, Xu J, Murphy S (2008) Deaths: Final data for 2005. *Natl Vital Stat Rep* 56:5.
28. Guyton, AC, Hall, JE (2006) *Textbook of Medical Physiology* (Elsevier Saunders, Philadelphia), 11th Ed.
29. Costanzo, L (2002) *Physiology* (Saunders, Philadelphia), 2nd Ed.
30. Bullock J, Boyle J, Wang MB (2004), *Physiology* (Lippincott Williams and Wilkins, Philadelphia) 2nd Ed.
31. Avtar R, Tandon D (2007) Modelling the transmural transport of oxygen to the retina. *Appl Math Comput* 186:540–547.
32. Lubkin S, Jackson T (2002) Multiphase mechanics of capsule formation in tumors. *J Biomech Eng* 124:237–243.
33. Grote J, Susskind R, Vaupel P (1977) Oxygen diffusivity in tumor tissue (ds-carcinosarcoma) under temperature conditions within the range of 20 40 c. *Eur J Physiol* 372:37–42.